 CMC, vol.53, no.1, pp.1-22, 2017

Forced and Natural Vibrations of an Orthotropic Pre-Stressed Rectangular Plate with Neighboring Two Cylindrical Cavities

U. Babuscu Yesil[1]

Abstract: Forced and natural vibrations of a rectangular pre-stressed orthotropic composite plate containing two neighboring cylindrical cavities whose cross sections are rectangular with rounded-off corners are investigated numerically. It is assumed that all the end surfaces of the rectangular pre-stressed composite plate are simply supported and subjected to a uniformly distributed normal time-harmonic force on the upper face plane. The considered problem is formulated within the Three-Dimensional Linearized Theory of Elastic Waves in Initially Stressed Bodies (TDLTEWISB). The influence of mechanical and geometrical parameters as well as the initial stresses and the effect of cylindrical cavities on the dynamical characteristics of the rectangular orthotropic composite plate are analyzed and discussed.

Keywords: Initial stresses, vibration, cylindrical cavities, 3D FEM, orthotropic material.

1 Introduction

Many defects such as holes and cavities within structural elements subjected to external effects are responsible for the stress concentrations around them. Knowledge of the magnitude of these stress concentrations is necessary to safely use these structural elements containing holes or cavities in engineering structures. This is because the values of the stress concentrations in the case where they are close to their critical value can cause a variety of dangerous situations in structures containing such defects to arise. A wide range of research in this area has been made and continues to be studied intensively in many branches of science. These problems were extensively studied, firstly by Savin [Savin (1961)]. Since then, many aspects of these problems have been developed by many researchers such as the considered structural elements and their materials, solution methods and the theories used in the mathematical modeling of these problems. Stress concentration around two cylindrical horizontal holes in a rectangular plate was investigated in [Akbarov, Yahnioglu and Babuscu (2012)], Weakening Effects of Internal Part-Through Elliptic Holes in Homogeneous and Laminated Composite Plates was investigated in [Chaudhuri (2007)]. A method of finding the general solution of a system of equilibrium equations for nonthin transversely isotropic plates with a uniform pre-stress field was investigated in [Khoma and Kondratenko (2008)]. A non-contact measurement method was investigated to investigate the tensile strain field of a composites plate in the

[1] Department of Mathematical Engineering, Faculty of Chemical and Metallurgical Eng., Yildiz Technical University, Davutpasa Campus, 34210, Esenler, Istanbul, Turkey.
E-mail: ubabuscu@yildiz.edu.tr

presence of stress concentrations caused by a geometrical defect consisting of circular hole in [Toubal, Karama and Lorrai (2005)]. A single-layer higher-order model for predicting the stresses at curved free boundaries of laminated composite plates subjected to inplane loading was investigated in [Zhen and Wanji (2009)]. In [Zheng, Chang-Boo, Chongdu and Hyeon (2008)] the coupled influence of the Poisson's ratio and plate thickness upon the stress concentration factor, the strain concentration factor and their relations of finite thickness plate containing a hole subjected to uniaxial tension were vastly investigated using the finite element method.

In these works consideration was given to determination of the values of the stress and strain concentrations around the holes and the effects of the geometrical and material parameters on them. However, in some research, holes which were seen as being responsible for the stress concentration under loading were used for reduction of the stress concentration around the discontinuities i.e. around the other holes. An overview of various techniques developed for analysis as well as the mitigation of stress concentration in plates with singularities is given by S. Nagpal et al. [Nagpal, Jain and Sanyal (2012)]. But all the above-mentioned research is related to the corresponding problem in the static case. However, it has been established that stress concentrations significantly affect the dynamical characteristics of plates containing holes. The forced vibration of an initially statically stressed rectangular plate made of an orthotropic material with a cylindrical hole was investigated in [Akbarov, Yahnioglu and Babuscu (2010)]. An analysis of the forced vibration of an initially stressed rectangular transversally isotropic plate containing two neighboring cylindrical cavities was investigated in [Akbarov, Yahnioglu and Babuscu Yesil (2012)]. Coupling method was investigated for free vibration analyses of rectangular plate with a rectangular or circular hole in [Kwaka and Han (2007)]. Free vibration analysis of composite plates in the presence of cutouts undergoing large amplitude oscillations was investigated in [Sivakumar and Iyengar (1999)]. Stress distribution in the pre-stretched simply supported strip containing two neighbouring circular holes under forced vibration was investigated in [Yahnioglu (2007)]. The influence of the initial stretching of a composite thick plate containing a cylindrical hole on the stress concentration around a hole caused by the action of the additional uniformly distributed dynamic (time-harmonic) normal forces on the upper face of the plane was investigated in [Yahnioglu and Babuscu (2009)]. The first aim is to determine the magnitude of the stress concentrations around the defects; the second aim is to find ways of reduction for these concentrations. One way to reduce the values of the stress concentrations around the defects is the use of pre-stressed materials in elements of structures with defects. The effects of initial stresses on the stress concentration around holes were investigated in some papers as mentioned above.

The present study extends the study [Akbarov, Yahnioglu and Babuscu (2010)] for the case where the pre-stressed orthotropic rectangular plate contains two equal internal parallel neighboring cylindrical cavities (lying width-wise in the plate) with rectangular cross sections with rounded corners. And the present study extends the study [Akbarov, Yahnioglu and Babuscu (2012)] by taking the plate's material as orthotropic and extends the study [Akbarov, Yahnioglu and Babuscu (2012)] by examining the dynamical characteristics of the plate. Mathematical modeling is made within the TDLTEWISB and according to this theory, initial stress distributions are determined in the considered plate by employing the linear elasticity theory and then, using the equations and relations of

the TDLTEWISB containing the initial stress distributions in the plate, the forced and natural vibrations of the pre-stressed rectangular orthotropic plate are investigated. It is assumed that the initial stresses are caused by the uniformly distributed normal forces acting on two opposite end-planes which are normal to the direction in which the cylindrical cavities lie. Both determination of the initial stresses and the dynamical quantities such as the fundamental frequencies and stress concentrations under vibration of the considered rectangular plate are calculated numerically by using 3D finite element modeling. The influence of the geometrical and mechanical parameters of the orthotropic plate and interaction between the cavities, as well as the initial stresses on the dynamical characteristics of the considered plate are analyzed and discussed.

2 Formulation of the problem

Consider a rectangular orthotropic plate containing two equal parallel cylindrical cavities whose cross sections are rectangular with rounded-off corners, the geometries of which are shown in Fig. 1, and according to which, the plate's height, length and thickness are h, ℓ_1 and ℓ_3, respectively. Determine the position of the points by the Lagrange coordinates which, in the natural state, coincide with the Cartesian coordinates $Ox_1x_2x_3$. Assume that the cylindrical cavities extend longitudinally along the thickness ℓ_3.

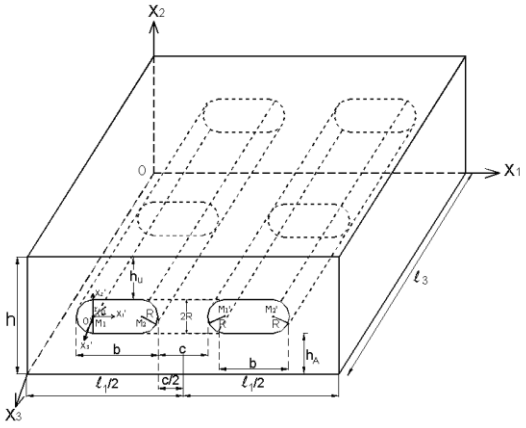

Figure 1: The geometry of the considered rectangular plate including two equal cylindrical cavities

In the considered problem, the solution domain occupies the region:

$$\Omega' = \left(\Omega - \Omega_{\mathrm{I}} - \Omega_{\mathrm{II}}\right) \tag{1}$$

In (1) the domain Ω_{I} (Ω_{II}) is occupied by the left (right) cylindrical cavity and the following notation is used:

$$\Omega = \left\{0 \le x_1 \le \ell_1; 0 \le x_2 \le h; 0 \le x_3 \le \ell_3\right\}$$

$$\Omega_{\mathrm{I}} = \left\{ \mathrm{x}_{01} \le \mathrm{x}_1 \le \left(\mathrm{x}_{01} + \mathrm{b} - 2\mathrm{R}\right); \mathrm{y}_{01} - \mathrm{R} \le \mathrm{x}_2 \le \mathrm{y}_{01} + \mathrm{R}; 0 \le \mathrm{x}_3 \le \ell_3 \right\} \cup$$

$$\left\{(x_1,x_2,x_3)\middle|(x_1-x_{01})^2+(x_2-y_{01})^2\le R^2,(x_{01}-R)\le x_1\le x_{01};y_{01}-R\le x_2\le y_{01}+R;0\le x_3\le \ell_3\right\}\cup$$
$$\left\{(x_1,x_2,x_3)\middle|(x_1-x_{02})^2+(x_2-y_{02})^2\le R^2,\ x_{02}\le x_1\le x_{02}+R;y_{01}-R\le x_2\le y_{01}+R;0\le x_3\le \ell_3\right\}$$
$$\Omega_{II}=\left\{x'_{01}\le x_1\le (x'_{01}+b-2R);y'_{01}-R\le x_2\le y'_{01}+R;0\le x_3\le \ell_3\right\}\cup$$
$$\left\{(x_1,x_2,x_3)\middle|(x_1-x'_{01})^2+(x_2-y'_{01})^2\le R^2,(x'_{01}-R)\le x_1\le x'_{01};y'_{01}-R\le x_2\le y'_{01}+R;0\le x_3\le \ell_3\right\}\cup$$
$$\left\{(x_1,x_2,x_3)\middle|(x_1-x'_{02})^2+(x_2-y'_{02})^2\le R^2,\ x'_{02}\le x_1\le (x'_{02}+R);y'_{01}-R\le x_2\le y'_{01}+R;0\le x_3\le \ell_3\right\} \tag{2}$$

where (x_{01},y_{01}) ((x_{02},y_{02})) is the center of the left (right) half circular arc of the first cavity near the left side of the plate and (x'_{01},y'_{01}) ((x'_{02},y'_{02})) is the center of the left (right) half circular arc of the second cavity near the right side of the plate. Suppose that at first, this plate is stretched (or compressed) by the uniformly distributed normal static forces with intensity q acting on the $x_1=0$ and $x_1=\ell_1$ planes (Fig. 2.b). Next, suppose that additional uniformly distributed dynamic (time-harmonic) normal forces with intensity p are applied on the plane $x_2=h$. (Fig 2.c) These loading stages are shown in Fig. 2 schematically. Note that within this study our aim is to determine the effects of the initial stressed state on the stressed state caused by the additional force. Therefore, the superposition principle is not applicable. Assume that $p\ (<<q)$. Henceforth all the quantities referring to the initial state will be labeled by the superscript (0) and the repeated indices in equations are summed over their ranges.

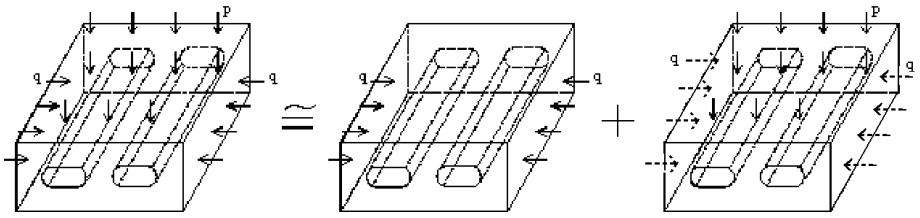

(a) (b) (c)

Figure 2: Loading of the considered rectangular plate including two equal cylindrical cavities

According to the above discussion, to determine the initial stress-state, the following boundary-value problem can be solved.

Equilibrium equations:

$$\frac{\partial\sigma_{ij}^{(0)}}{\partial x_j}=0 \tag{3}$$

Mechanical Relations:

$$\boldsymbol{\sigma}^{(0)}=\mathbf{D}\boldsymbol{\varepsilon}^{(0)},\left(\boldsymbol{\sigma}^{(0)}\right)^{\mathrm{T}}=\left(\sigma_{11}^{(0)}\ \sigma_{22}^{(0)}\ \sigma_{33}^{(0)}\ \sigma_{23}^{(0)}\ \sigma_{13}^{(0)}\ \sigma_{12}^{(0)}\right),$$

$$\left(\boldsymbol{\varepsilon}^{(0)}\right)^{\mathrm{T}}=\left(\varepsilon_{11}^{(0)}\ \varepsilon_{22}^{(0)}\ \varepsilon_{33}^{(0)}\ \varepsilon_{23}^{(0)}\ \varepsilon_{13}^{(0)}\ \varepsilon_{12}^{(0)}\right) \tag{4}$$

Geometrical Relations:

$$\varepsilon_{ij}^{(0)}=\frac{1}{2}\left(\frac{\partial u_i^{(0)}}{\partial x_j}+\frac{\partial u_j^{(0)}}{\partial x_i}\right) \tag{5}$$

Boundary Conditions:

$$u_2^{(0)}\Big|_{x_1=0;\ell_1}=u_2^{(0)}\Big|_{x_3=0;\ell_3}=0,\ \sigma_{1i}^{(0)}\Big|_{x_1=0;\ell_1}=q\delta_1^i,\ \sigma_{2i}^{(0)}\Big|_{x_2=0;h}=0,$$

$$\sigma_{31}^{(0)}\Big|_{x_3=0;\ell_3}=\sigma_{33}^{(0)}\Big|_{x_3=0;\ell_3}=0,\ \sigma_{ij}^{(0)}n_j^{(I)}\Big|_{S_I}=0,\ \sigma_{ij}^{(0)}n_j^{(II)}\Big|_{S_{II}}=0\ \ i;j=1,2,3 \tag{6}$$

In Eq. (6) S_I (S_{II}) shows the surface of the first (the second) cylindrical cavity and $n_j^{(I)}$ ($n_j^{(II)}$) are the components of the unit's outward normal vector to the surface S_I (S_{II}) in (6).

To determine the stress-state caused by additional dynamic loading, the following boundary-value problem must be solved.

TDLTEWISB equations of motion [Akbarov, Yahnioglu and Babuscu (2012), Guz (2004)]:

$$\frac{\partial}{\partial x_j}\left(\sigma_{ji}+\sigma_{in}^{(0)}\frac{\partial u_i}{\partial x_n}\right)=\rho\frac{\partial^2 u_i}{\partial t^2} \tag{7}$$

Mechanical relations

$$\boldsymbol{\sigma}=\mathbf{D}\boldsymbol{\varepsilon},\ \left(\boldsymbol{\sigma}\right)^{\mathrm{T}}=\left(\sigma_{11}\ \sigma_{22}\ \sigma_{33}\ \sigma_{23}\ \sigma_{13}\ \sigma_{12}\right),\ \left(\boldsymbol{\varepsilon}\right)^{\mathrm{T}}=\left(\varepsilon_{11}\ \varepsilon_{22}\ \varepsilon_{33}\ \varepsilon_{23}\ \varepsilon_{13}\ \varepsilon_{12}\right), \tag{8}$$

Geometrical relations:

$$\varepsilon_{ij}=\frac{1}{2}\left(\frac{\partial u_i}{\partial x_j}+\frac{\partial u_j}{\partial x_i}\right) \tag{9}$$

Boundary conditions:

$$u_2\Big|_{x_1=0;\ell_1}=u_2\Big|_{x_3=0;\ell_3}=0,\ \left(\sigma_{j1}+\sigma_{1n}^{(0)}\frac{\partial u_1}{\partial x_n}\right)n_j\Big|_{x_1=0;\ell_1}=\left(\sigma_{j3}+\sigma_{3n}^{(0)}\frac{\partial u_3}{\partial x_n}\right)n_j\Big|_{x_1=0;\ell_1}=0,$$

$$\left(\sigma_{jk}+\sigma_{kn}^{(0)}\frac{\partial u_k}{\partial x_n}\right)n_j\Big|_{x_2=h}=pe^{i\omega t},\ \left(\sigma_{ji}+\sigma_{in}^{(0)}\frac{\partial u_i}{\partial x_n}\right)n_j\Big|_{x_2=0}=0,$$

$$\left(\sigma_{j1}+\sigma_{1n}^{(0)}\frac{\partial u_1}{\partial x_n}\right)n_j\Big|_{x_3=0;\ell_3}=\left(\sigma_{j3}+\sigma_{3n}^{(0)}\frac{\partial u_3}{\partial x_n}\right)n_j\Big|_{x_3=0;\ell_3}=0,$$

$$\left(\sigma_{ji}+\sigma_{in}^{(0)}\frac{\partial u_i}{\partial x_n}\right)n_j^{(I)}\Big|_{S_I}=0,\left(\sigma_{ji}+\sigma_{in}^{(0)}\frac{\partial u_i}{\partial x_n}\right)n_j^{(II)}\Big|_{S_{II}}=0\quad \text{i;j;k=1,2,3.} \tag{10}$$

In (7) - (10) conventional notation is used. It is assumed that the plate material is an orthotropic one with elastic symmetry axes Ox_1, Ox_2 and Ox_3. So matrix **D** in (4) and (8) is given as follows:

$$\mathbf{D}=\begin{Vmatrix} A_{11} & A_{12} & A_{13} & 0 & 0 & 0\\ A_{12} & A_{22} & A_{23} & 0 & 0 & 0\\ A_{13} & A_{23} & A_{33} & 0 & 0 & 0\\ 0 & 0 & 0 & 2A_{44} & 0 & 0\\ 0 & 0 & 0 & 0 & 2A_{55} & 0\\ 0 & 0 & 0 & 0 & 0 & 2A_{66} \end{Vmatrix} \tag{11}$$

where, according to [Christensen (1979)],

$$A_{ij}=\frac{(-1)^{i+j}a_{ij}}{\det\|a_{nm}\|},\ a_{11}=\frac{1}{E_1},\ a_{12}=\frac{-\nu_{12}}{E_2},\ a_{13}=\frac{-\nu_{13}}{E_3},\ a_{23}=\frac{-\nu_{23}}{E_3},$$

$$a_{22}=\frac{1}{E_2},\ a_{33}=\frac{1}{E_3},\ a_{ij}=a_{ji}\ ;\ G_{ij}=\mu_{ij}\ (\text{for } i\neq j),\ \text{i;j=1,2,3}. \tag{12}$$

In (12) E_1, E_2 and E_3 are the modules of elasticity of the plate material in the direction of the Ox_1, Ox_2 and Ox_3 axes, respectively, and υ_{12}, υ_{13} and υ_{23} are Poisson's ratios for this material. G_{12}, G_{13}, and G_{23}, denote the shear modulus of the plate material in the Ox_1x_2, Ox_1x_3 and Ox_2x_3 planes, respectively. Since the applied additional loading is time-harmonic and the steady state is considered, then all the dependent variables are also time-harmonic and can be represented as follows:

$$\left\{\sigma_{ij},\varepsilon_{ij},u_i\right\}=\left\{\bar{\sigma}_{ij},\bar{\varepsilon}_{ij},\bar{u}_i\right\}\exp(i\omega t) \tag{13}$$

where the quantities with over-bars denote the amplitude of the corresponding quantities. For simplicity, below it is omitted these over-bars. Substituting expression (13) into Eq. (7) - (10) and doing some manipulations, the following equation in terms of the amplitude of the corresponding quantities is obtained:

$$\frac{\partial}{\partial x_j}\left(\bar{\sigma}_{ji}+\sigma_{in}^{(0)}\frac{\partial \bar{u}_i}{\partial x_n}\right)+\rho\omega^2\bar{u}_i=0 \tag{14}$$

and the boundary condition in (10) at $x_2=h$ is replaced with the following one:

$$\left(\bar{\sigma}_{jk} + \sigma_{kn}^{(0)} \frac{\partial \bar{u}_k}{\partial x_n} \right) n_j \Big|_{x_2 = h} = p\delta_2^k \tag{15}$$

The other boundary conditions and relations are identically satisfied for the corresponding amplitude of the sought values. In (15), δ_i^j is the Kronecker symbol.

Eventually, the investigation of the boundary value problem of the stress-state caused by additional dynamic loading is reduced to the solution of the boundary value problem given in Eqs. (8) - (10), (14) and (15). Note that the case where $p = 0$ in (15) corresponds to the natural vibration problem of the plate under consideration. Thus, the mathematical formulation of the considered problem is fully defined.

3 Solution method: finite element formulation

The foregoing boundary value problems will be investigated by employing 3D FEM modeling. The displacement-based finite elements for the FEM modeling is used. It means that unknown values at each node of a finite element are selected displacements only [Zienkiewicz and Taylor (1989)]. For this purpose, for the FEM modeling of the boundary value problem in (3) - (6), the functional

$$\Pi^{(0)} = \frac{1}{2} \iiint_{\Omega'} \sigma_{ij}^{(0)} \varepsilon_{ij}^{(0)} d\Omega' - \iint_{S_q} \sigma_{ij} n_j u_i dS_q = \frac{1}{2} \iiint_{\Omega'} \sigma_{ij}^{(0)} \varepsilon_{ij}^{(0)} d\Omega' + \int_0^h \int_0^{\ell_3} q u_1^{(0)} \Big|_{x_1=0} dx_2 dx_3 - \int_0^h \int_0^{\ell_3} q u_1^{(0)} \Big|_{x_1=\ell_1} dx_2 dx_3 \tag{16}$$

is introduced and for the FEM modeling of the problem (8) - (10), (14) and (15) the functional

$$\Pi = \frac{1}{2} \iiint_{\Omega`} \left(T_{ij} \frac{\partial \bar{u}_j}{\partial x_i} + \rho\omega^2 \bar{u}_i \bar{u}_j \right) d\Omega - \iint_{S_p} T_{ij} n_j \bar{u}_i dS_p \tag{17}$$

is introduced, where Ω' is the solution domain determined by expressions (1) and (2). Moreover, in (17) the following notation is used:

$$T_{ij} = \bar{\sigma}_{ij} + \sigma_{ij}^{(0)} \frac{\partial \bar{u}_i}{\partial x_n} \tag{18}$$

where $\sigma_{ij}^{(0)}$ are the components of the initial stresses determined from the solution to the boundary value problem (3) - (6). For each functional, using the virtual work principle and employing the well-known Ritz technique, FEM modeling for each problem is obtained. Note that from the equations $\delta\Pi^{(0)} = 0$ and $\delta\Pi = 0$, i.e. from the first variations of these functionals, the governing equations and boundary conditions with respect to the stresses for the boundary value problems (3)-(6) and (8)-(10), (14) and (15) are obtained, respectively. In this way, the validity of the functionals (16) and (17) for the FEM modeling of the considered problems is proved.

Only one quarter of the region is considered under FEM modeling, since the problem is symmetric with respect to the $x_1 = \ell_1/2$ and $x_3 = \ell_3/2$ planes (Fig. 3). In this case, the surroundings of the cylindrical cavities are modeled by triangular prism finite elements. For the remaining part of the region not covered by the triangular prism finite elements, rectangular prism (brick) elements are used. Triangular prism finite elements have six corner nodes and rectangular prism (brick) finite elements have eight corner nodes. The selection of the number degrees of freedom (NDOF) is determined from the requirements that the boundary conditions should be satisfied with very high accuracy and the numerical results obtained for various NDOFs must converge. In accordance with the finite elements method, the solution domain Ω' is divided into a finite number of finite elements as follows:

$$\Omega' = \bigcup_{k=1}^{M} \Omega'_k \tag{19}$$

where Ω'_k shows the k-th finite element (Fig. 3).

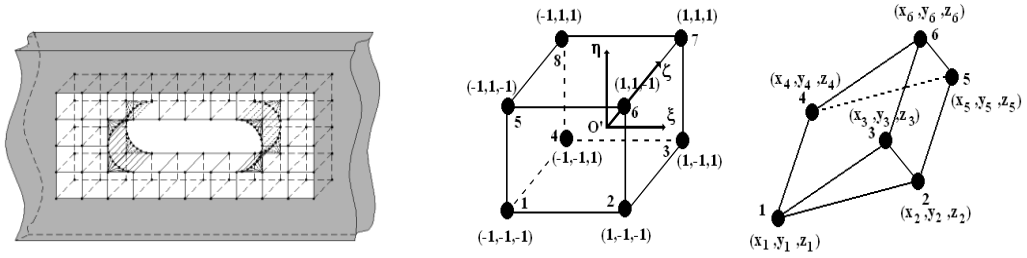

(a) (b)

Figure 3: a) The finite elements mesh around the cylindrical cavity;

b) The geometry of the brick and the triangular prism finite elements.

For the solution to the considered boundary value problems, the functions of the displacements in each finite element are determined as polynomial functions in terms of shape functions and unknown values of the displacement at the nodes of that element.

$$u^{(k)} \approx N^{(k)} a^{(k)},\ k=1,2,\ldots,M \tag{20}$$

where

$$\left(a^{(k)}\right)^T = \left\{u_{11}^k, u_{21}^k, u_{31}^k, u_{12}^k, u_{22}^k, u_{32}^k \ldots, u_{1p}^k, u_{2p}^k, u_{3p}^k\right\},$$

$$\left(N^{(k)}\right)^T = \begin{Bmatrix} N_1^k & 0 & 0 & N_2^k & 0 & 0 & \ldots & N_p^k & 0 & 0 \\ 0 & N_1^k & 0 & 0 & N_2^k & 0 & \ldots & 0 & N_p^k & 0 \\ 0 & 0 & N_1^k & 0 & 0 & N_2^k & \ldots & 0 & 0 & N_p^k \end{Bmatrix},$$

$$\left(u^{(k)}\right)^T = \left\{u_1^k(x_1,x_2,x_3), u_2^k(x_1,x_2,x_3), u_3^k(x_1,x_2,x_3)\right\}. \tag{21}$$

In Eq. (21) p equals 8 (6) for a brick (a triangular prism) finite element. For the rectangular finite element, the second-order standard Lagrange-family shape functions are used at nodes in normalized coordinates [Zienkiewicz and Taylor (1989)]. For calculating the shape functions of triangular prism finite elements, triangular pyramids are used. For this purpose each triangular prism element divided into three triangular pyramidal elements (Fig. 4)

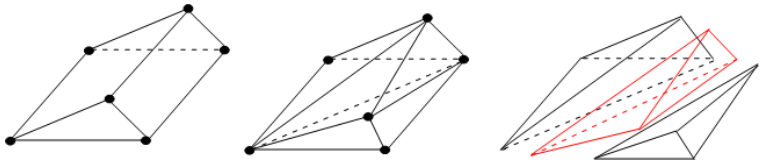

Figure 4: Separation of triangular prism elements into triangular pyramidal finite elements

Volume coordinates L_i (i=1,2,3,4) with the help of a moving point $p(x,y,z)$ in volume are determined for calculating the shape functions of triangular prism finite elements (Fig. 5).

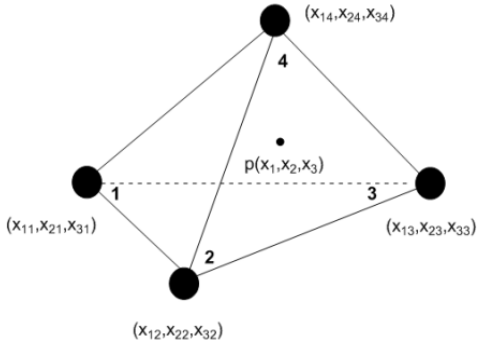

Figure 5: Triangular pyramidal finite elements

$$N_i^{(k)}(x,y,z) = L_i^{(k)},\ L_i^{(k)} = \frac{V_i^{(k)}}{V^{(k)}} \tag{22}$$

In (22) $V^{(k)}$ shows the volume of the k-th tri-angular pyramidal elements. The relations between volume coordinates and Cartesian coordinates:

$$x_1 = x_{11}L_1 + x_{12}L_2 + x_{13}L_3 + x_{14}L_4;$$

$$x_2 = x_{12}L_1 + x_{22}L_2 + x_{23}L_3 + x_{24}L_4;$$

$$x_3 = x_{31}L_1 + x_{32}L_2 + x_{33}L_3 + x_{34}L_4;$$

$$1 = L_1 + L_2 + L_3 + L_4 \tag{23}$$

Substituting Eq. (20) into Eq. (16) and Eq. (17), after some mathematical manipulations, finally yields the following system of algebraic equations are obtained as follows:

The system for the algebraic equation for the first boundary value problem ((3)-(6))

$$\mathbf{K}^{(0)}\mathbf{a}^{(0)} = f^{(0)} \tag{24}$$

and the system for the algebraic equation for the second boundary value problem ((8)-(10), (14) and (15))

$$\left(\mathbf{K} - \omega^2\mathbf{M}\right)\mathbf{a} = f \tag{25}$$

are obtained respectively, where $\mathbf{K}^{(0)}$ and $\mathbf{K}$ are the stiffness matrices, $\mathbf{M}$ is the mass matrix, $\mathbf{a}^{(0)}$ and $\mathbf{a}$ are the vectors whose components are values of the unknown displacements at selected nodes, and $\boldsymbol{f}^{(0)}$ and $\boldsymbol{f}$ are the force vectors [Akbarov S.D.,Guz A.N. (2000), Zienkiewicz O.C., Taylor R.L. (1989)]. The values of these matrices for k-th finite element (Ω_k**)**:

$$K_{ijk}^{(0)} = \iiint\limits_{\Omega_k}\left(B_j^{(k)}\right)^T D^{(k)} B_i^{(k)} d\Omega_k, \quad \begin{matrix} i; j = 1,2,...,p \\ k = 1,2,...,M \end{matrix} \tag{26}$$

$$B_j^{(k)} = \begin{pmatrix} \frac{\partial N_j}{\partial x_1} & 0 & 0 & \frac{\partial N_j}{\partial x_2} & 0 & \frac{\partial N_j}{\partial x_3} \\ 0 & \frac{\partial N_j}{\partial x_2} & 0 & \frac{\partial N_j}{\partial x_1} & \frac{\partial N_j}{\partial x_3} & 0 \\ 0 & 0 & \frac{\partial N_j}{\partial x_3} & 0 & \frac{\partial N_j}{\partial x_2} & \frac{\partial N_j}{\partial x_1} \end{pmatrix}, \; j=1,2,\ldots,p \tag{27}$$

$$M_{ijk}^{(1)} = \iiint\limits_{\Omega_k} N_j^T N_i d\Omega_k \tag{28}$$

The solutions to Eqs. (24) and (25) give the values of the displacements at each node. However, equation (25) includes the values of the stresses obtained from the solution to the first boundary value problem. So, before finding the solution to Eq. (25), the distribution of the stresses for the first boundary value problem should be found. Using the solution to Eq. (24) and Hooke's Law, they are obtained. Furthermore, the fundamental frequency of the considered plate can be determined from equation:

$$\det\left|\mathbf{K} - \omega^2\mathbf{M}\right| = 0 \tag{29}$$

Note that the same number of finite elements is taken and the same arrangements are used for the FEM modeling in obtaining the numerical solutions of the considered problems. The normalized coordinates for the brick finite elements and Gauss quadrature method are used for the calculation of the numerical integrals with ten sample points in each finite element. Volume coordinate for the triangular prism finite elements is used and numerical integrals are calculated with formula (30) for triangular pyramidal finite elements [Zienkiewicz and Taylor (1989)].

$$\iiint_V L_1^a L_2^b L_3^c L_4^d dx dy dz = \frac{a!b!c!d!}{(a+b+c+d+3)!} 6V \tag{30}$$

In (30), L_i (i=1,2,3,4) are the components of volume coordinates, (a,b,c,d) are the degree of these components and V is the volume of the pyramidal elements

Thus, the discussion above completes consideration of the FEM modeling of the formulated problem.

4 Numerical results and discussions

The primary focus of the present study analyzes the effect of the initial stresses and the effect of the interaction between two cylindrical cavities on the natural and forced vibration of an orthotropic rectangular plate. Numerical results are presented for orthotropic composite rectangular plates with two neighboring cylindrical cavities. The material properties of the considered plate are represented by the parameters $E_1, E_2, E_3, G_{12}, G_{13}, G_{23}, \upsilon_{12}, \upsilon_{13}$ and υ_{23} Here, the symbols E_i, G_{ij} and υ_{ij} (i=1,2,3) represent the modulus of elasticity, Shear modulus and Poisson's ratio of the considered material, respectively.

Since the considered boundary value problems and the solution domain (1) have symmetry with respect to the $x_1 = \ell_1/2$ and $x_3 = \ell_3/2$ planes, these symmetry conditions permit us to make finite element modeling in a quarter of the plate (see Fig. 1). This part of the plate (solution domain) is divided into 30, 12 and 30 brick elements along the direction of the Ox_1, Ox_2 and Ox_3 axes respectively, but 32 triangular prism finite elements are used around the single cavity in a layer. Hence, 10200 brick and 960 triangular prism finite elements, 13082 nodes and 37596 NDOFs have been used in total for the FEM modeling. Note that all the algorithms and programs required for the numerical solutions of the considered boundary value problems using the finite element method are implemented in a FORTRAN code composed by the author.

The dimensionless parameter of frequency $\bar{\omega}^2$ ($= \omega^2 \rho \ell_1 / A_{22}$) is introduced, through which the frequency of the additional external forces is estimated. It is characterized the intensity of the initial forces through the parameter q/E_1 and analyze the concentration of the stresses around the cylindrical cavities in the cylindrical coordinate system $O'r\theta x_3'$ (Fig. 1).

In order to see the validity of the algorithm and programs which are composed by the author, first, the values of the fundamental natural frequencies ($\bar{\omega}_{cr}^2$) for the whole plate (i.e. the plate without cavities) are calculated. Assume that the plate material consists of alternating two isotropic layers with mechanical constants E_k (Young's modulus) and ν_k (Poisson's ratio) ($k = 1, 2$) [Akbarov (2000)]. According to the well-known mechanical consideration, the values of $\bar{\omega}_{cr}^2$ must approach the corresponding ones obtained for the plane-strain state i.e. with ℓ_3/ℓ_1. This prediction is proven by the data given in Table 1 which shows the values of

the fundamental frequency obtained for various ℓ_3/ℓ_1. It follows from this table that the values of $\bar{\omega}_{cr}^2$ decreases with ℓ_3/ℓ_1 and approach the corresponding values given in [Akbarov (2000)] obtained in the plane strain-state.

Table 1: The effect of ℓ_3/ℓ_1 on $\bar{\omega}_{cr}^2$ for the transversally isotropic rectangular plate without a cylindrical cavity where $q/E_1 = 0$, $h/\ell_1 = 0.10$ and $\upsilon_1 = \upsilon_2 = 0.3$. [Akbarov S.D., Yahnioglu N., Babuscu Yesil U. (2012), Akbarov S.D., Yahnioglu N., Babuscu Yesil U. (2012)]

E_2/E_1	ℓ_3/ℓ_1				Akbarov and Guz (2000)
	1	2	3	4	
1	0.23	0.09	0.08	0.07	0.06
10	0.56	0.24	0.21	0.19	-
20	0.93	0.41	0.35	0.33	0.31
50	1.92	0.80	0.70	0.67	0.62

Table 2 and Table 3 show the effect of the parameter b/R which characterizes the volume of the cylindrical cavities, and initial stretching force (q/E_1) on $\bar{\omega}_{cr}^2$ for transversely isotropic and orthotropic plates, respectively. If the values of the parameter b/R decreases, i.e. if the total volume of the cavities decreases, the values of $\bar{\omega}_{cr}^2$ approach a certain asymptote. The value of this asymptote is the value of $\bar{\omega}_{cr}^2$ for the corresponding plate without cavities [Akbarov (2000)]. In this way, the validity and reliability of the algorithm and programs used are also proved.

Unless otherwise specified, we assume that $\nu_{12} = \nu_{13} = \nu_{23} = 0.3$, $h/\ell_1 = 0.10$, $R/\ell_1 = 0.00833$, and $\ell_3/\ell_1 = \gamma_{31} = 1$ for obtaining the following numerical results. The values of the other parameters are given in the tables or in the figures.

Table 2: The effect of b/R on $\bar{\omega}_{cr}^2$ for a transversely isotropic plate with two cylindrical cavities in the case where $h/\ell_1 = 0.10$, $\gamma_{31} = \ell_3/\ell_1 = 1$, $h_A/R = h_U/R = 5$, $\mathrm{R} = \mathrm{h}/12$, $\upsilon = 0.3$ and $\mathrm{c}/\mathrm{R} = 11$ [Akbarov S.D., Yahnioglu N., Babuscu Yesil U. (2012), Akbarov S.D., Yahnioglu N., Babuscu Yesil U. (2012)].

q/E_1	E_2/E_1	b/R				
		22.00	15.00	13.00	6.25	0
0	1	0.271	0.259	0.249	0.239	0.238
	10	0.634	0.607	0.586	0.567	0.566
0.001	1	0.285	0.274	0.263	0.250	0.245

	10	0.643	0.617	0.594	0.572	0.570
0.005	1	0.339	0.334	0.317	0.297	0.274
	10	0.680	0.654	0.628	0.598	0.586

Table 3: The effect of b/R on $\bar{\omega}_{cr}^2$ for an orthotropic plate with two cylindrical cavities in the case where $h/\ell_1 = 0.10$, $c/R = 7.75$, $\gamma_{31} = \ell_3/\ell_1 = 1$, $h_A/R = h_U/R = 5$, $R = h/12$, $\upsilon_{12} = \upsilon_{13} = \upsilon_{23} = 0.3$, $E_2/E_1 = E_3/E_1 = 0.5$ and $G_{12}/E_1 = G_{13}/E_1 = G_{23}/E_1 = 0.1$.

q/E_1	b/R				
	22.00	13.00	8.50	6.25	0.00
0	0.279	0.230	0.220	0.219	0.218
0.005	0.372	0.333	0.319	0.280	0.272
0.010	0.459	0.410	0.394	0.353	0.325

Table 4: The effect of c/R on $\bar{\omega}_{cr}^2$ for an orthotropic plate with two cylindrical cavities in the case where $h_A/R = h_U/R = 5$, $G_{12}/E_1 = G_{13}/E_1 = G_{23}/E_1 = 0.1$, $E_2/E_1 = E_3/E_1 = 0.5$ and $b/R = 22.00$.

q/E_1	c/R					
	A centered Single Cavity	3.25	5.50	7.75	14.50	21.25
0	0.186	0.246	0.252	0.279	0.307	0.347
0.005	0.258	0.353	0.358	0.372	0.402	0.441
0.010	0.327	0.435	0.439	0.459	0.492	0.531

The values given in Table 4 show the effect of the interaction between the cavities, i.e., the effect of the parameter c/R on $\bar{\omega}_{cr}^2$ where $h_U/R = h_A/R = 5$, $G_{12}/E_1 = G_{13}/E_1 = G_{23}/E_1 = 0.1$, $E_2/E_1 = E_3/E_1 = 0.5$ and $b/R = 22.00$. It is concluded that when two cavities are close to each other, the fundamental natural frequencies decrease. Table 4 also shows that the initial stretching force causes an increase in the values of $\bar{\omega}_{cr}^2$. In Table 5, the values of $\bar{\omega}_{cr}^2$ are given for the various values of E_2/E_1 and E_3/E_1 for the case where $G_{12}/E_1 = G_{13}/E_1 = G_{23}/E_1 = 0.1$, $h_U/R = h_A/R = 5$, $b/R = 22.00$. and $c/R = 7.75$. It can be concluded that the values of $\bar{\omega}_{cr}^2$ increases with E_3/E_1, but the values of $\bar{\omega}_{cr}^2$ decreases with E_2/E_1 .The values in Table 5 also show that under the considered case, the values of E_2/E_1 have a greater effect on the values of $\bar{\omega}_{cr}^2$ than that of E_2/E_1 .

Table 5: The effect of E_3/E_1 and E_2/E_1 on $\bar{\omega}_{cr}^2$ for $h_A/R = h_U/R = 5$, $b/R = 22.00$. $c/R = 7.75$ and $G_{12}/E_1 = G_{13}/E_1 = G_{23}/E_1 = 0.1$.

q/E_1	E_3/E_1			
	0.3		0.5	
	E_2/E_1			
	0.3	0.5	0.3	0.5
0	0.178	0.0154	0.379	0.279
0.005	0.234	0.203	0.501	0.372
0.010	0.285	0.249	0.613	0.459

Table 6: The effect of the shear modulus (G_{ij}/E_1) on $\bar{\omega}_{cr}^2$ for $E_2/E_1 = E_3/E_1 = 0.5$, $h_A/R = h_U/R = 5$, $b/R = 22.00$ and $c/R = 7.75$.

q/E_1	$G_{13}/E_1 = 0.1$ $G_{23}/E_1 = 0.1$			$G_{12}/E_1 = 0.1$ $G_{23}/E_1 = 0.1$			$G_{13}/E_1 = 0.1$ $G_{12}/E_1 = 0.1$		
	G_{12}/E_1			G_{13}/E_1			G_{23}/E_1		
	0.1	0.05	0.01	0.1	0.05	0.01	0.1	0.05	0.01
0	0.279	0.225	0.120	0.279	0.248	0.206	0.279	0.268	0.250
0.005	0.372	0.333	0.213	0.372	0.343	0.287	0.372	0.376	0.402
0.010	0.459	0.419	0.295	0.459	0.414	0.345	0.459	0.479	0.533

In Table 6 the values of $\bar{\omega}_{cr}^2$ are given for the various shear moduli i.e. for various G_{ij}/E_1 for the case where $E_2/E_1 = E_3/E_1 = 0.5$, $h_A/R = h_U/R = 5$, $b/R = 22.00$ and $c/R = 7.75$. The numerical results in this table show that the values of $\bar{\omega}_{cr}^2$ are influenced more by the values of G_{12}/E_1 (the shear modulus of the plate material in the plane Ox_1x_2) than those of the other shear moduli: G_{13}/E_1 (the shear modulus of the plate material in the plane Ox_1x_3) and G_{23}/E_1 (the shear modulus of the plate material in the plane Ox_2x_3) and decreases with a decrease in the shear modulus G_{ij}/E_1.

Two types of initial forces, i.e. an initial stretching ($q/E_1 \rangle 0$) and an initial compressing ($q/E_1 \langle 0$) force are considered in the numerical calculation. In Table 7 the values of $\bar{\omega}_{cr}^2$ are given for various values of the initial forces. It can be concluded that the values of $\bar{\omega}_{cr}^2$ increases (decreases) with the initial stretching (compressing) forces.

Table 7: The effect of the initial stresses (q/E_1) on $\bar{\omega}_{cr}^2$ for $E_2/E_1 = E_3/E_1 = 0.5$, $h_A/R = h_U/R = 5$, $G_{12}/E_1 = G_{13}/E_1 = G_{23}/E_1 = 0.1$, $b/R = 22.00$ and $c/R = 7.75$.

q/E_1	0.010	0.005	0.001	0.000	-0.001	-0.005	-0.010
$\bar{\omega}_{cr}^2$	0.459	0.372	0.298	0.279	0.260	0.181	0.077

Table 8: The effect of h_U/R on $\bar{\omega}_{cr}^2$ for various q/E_1 in the case where $E_2/E_1 = E_3/E_1 = 0.5$, $G_{12}/E_1 = G_{13}/E_1 = G_{23}/E_1 = 0.1$, $b/R = 22.00$ and $c/R = 7.75$.

q/E_1	h_U/R			
	5	4	3	2
0	0.279	0.278	0.274	0.266
0.005	0.372	0.345	0.311	0.260
0.010	0.459	0.406	0.342	0.248

In Table 8 the effect of the values of h_U/R on $\bar{\omega}_{cr}^2$ for various q/E_1 under $E_2/E_1 = E_3/E_1 = 0.5$, $G_{12}/E_1 = G_{13}/E_1 = G_{23}/E_1 = 0.1$, $b/R = 22.00$ and $c/R = 7.75$ are given. Note that the ratio h_U/R characterizes the distance between the upper surface of the cavities and the upper face plane of the considered plate. It can be concluded that the values of $\bar{\omega}_{cr}^2$ decreases with a decrease in the values of h_U/R.

Table 9: Influence of the parameter η obtained for various initial forces on the fundamental frequencies for $E_2/E_1 = E_3/E_1 = 0.5$, $G_{12}/E_1 = G_{13}/E_1 = G_{23}/E_1 = 0.1$, $b/R = 22.00$ and $c/R = 7.75$.

q/E_1	η (%)
0.010	64
0.005	33
0.001	7
-0.001	-7
-0.005	-35
-0.010	-72

Table 9 illustrates the values of the parameter η $(= \frac{\bar{\omega}^2_{cr.(q/E_1 \neq 0)} - \bar{\omega}^2_{cr.(q/E_1=0)}}{\bar{\omega}^2_{cr.(q/E_1=0)}} \times 100)$ where $\bar{\omega}^2_{cr.(q/E_1 \neq 0)}$ ($\bar{\omega}^2_{cr.(q/E_1=0)}$) indicates the value of the fundamental frequency for the case where $q/E_1 \neq 0$ ($q/E_1 = 0$). Note that the parameter η shows the degree of the influence of the initial force (q/E_1) on the fundamental frequencies. According to the data given in Table

9, a conclusion can be drawn on the amount of change in the values of the fundamental frequencies caused by the initial loading.

Fig. 6 shows the influence of the initial force (q/E_1) on the values of $\sigma_{\theta\theta}/p$ calculated for the case where $b/R=22.00$, $c/R=7.75$, $h_A/R=h_U/R=5$, $E_2/E_1=E_3/E_1=0.5$, $G_{12}/E_1=G_{13}/E_1=G_{23}/E_1=0.1$ and $\bar{\omega}^2=0.16$ for an orthotropic plate. It follows from these graphs that the initial compressive force has a much greater effect on the values of the stresses than the corresponding values of the initial stretching force. It is also concluded that an increase in the absolute values of q/E_1 under initial tension (compression) causes a decrease (an increase) in the absolute local maximum values of the stress $\sigma_{\theta\theta}/p$.

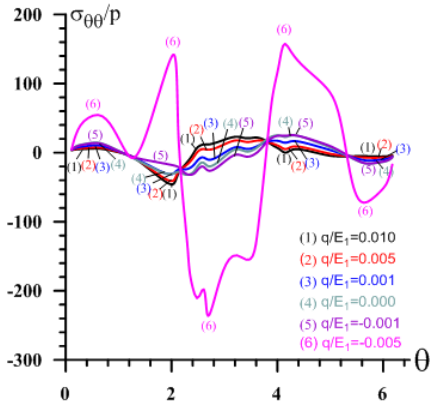

Figure 6: The distribution of $\sigma_{\theta\theta}/p$ with respect to θ under various initial forces q/E_1 in the case where $b/R=22.00$, $c/R=7.75$, $h_A/R=h_U/R=5$, $E_2/E_1=E_3/E_1=0.5$, $G_{12}/E_1=G_{13}/E_1=G_{23}/E_1=0.1$ and $\bar{\omega}^2=0.16$.

Fig. 7 shows the influence of the distance between the cavities along the Ox_1 axis i.e. the influence of the parameter c/R on the values of $\sigma_{\theta\theta}/p$ under $h/\ell=0.10$, $h_A/R=h_U/R=5$, $b/R=22.00$, $E_2/E_1=E_3/E_1=0.5$, $R/\ell_1=8.333*10^{-3}$, $G_{12}/E_1=G_{13}/E_1=G_{23}/E_1=0.1$ and $\bar{\omega}^2=0.16$ for an orthotropic plate. It follows from the graphs that in the considered case the absolute values of $\sigma_{\theta\theta}/p$ decreases monotonically with the distance between the cavities for $q/E_1=0.005$ but increases slightly with the distance between the cavities for $q/E_1=0$.

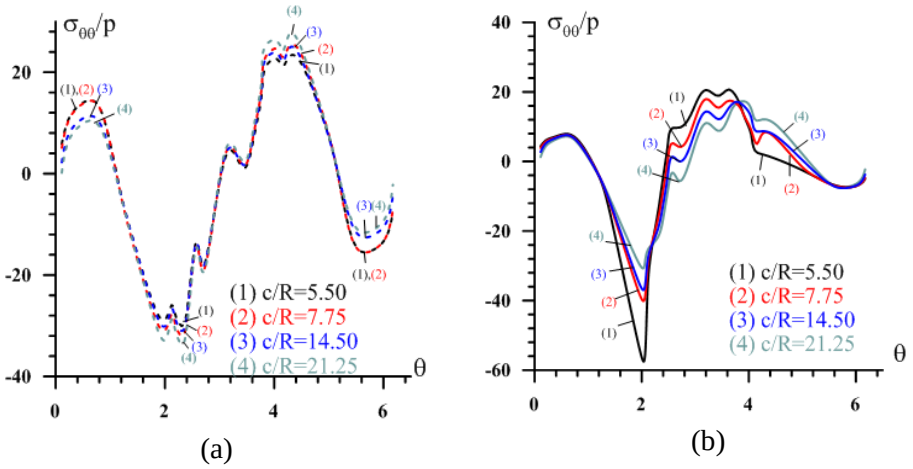

Figure 7: The distribution of $\sigma_{\theta\theta}/p$ with respect to θ under various distances between the cavities (c/R) for $q/E_1=0$ (a) and $q/E_1=0.005$ (b) in the case where

$b/R=22.00$, $h_A/R=h_U/R=5$, $E_2/E_1=E_3/E_1=0.5$,
$G_{12}/E_1=G_{13}/E_1=G_{23}/E_1=0.1$, and $\bar{\omega}^2=0.16$.

Fig. 8 shows the influence of the dimensionless frequency $\bar{\omega}^2$ on the values of $\sigma_{\theta\theta}/p$ in the case where $G_{12}/E_1=G_{13}/E_1=G_{23}/E_1=0.1$, $E_2/E_1=E_3/E_1=0.5$, $h_A/R=h_U/R=5$, $b/R=22.00$ and $c/R=7.75$. It follows from the graphs that the absolute values of $\sigma_{\theta\theta}/p$ increases monotonically with $\bar{\omega}^2$ for the cases where $q/E_1=0$ and $q/E_1\neq 0$.

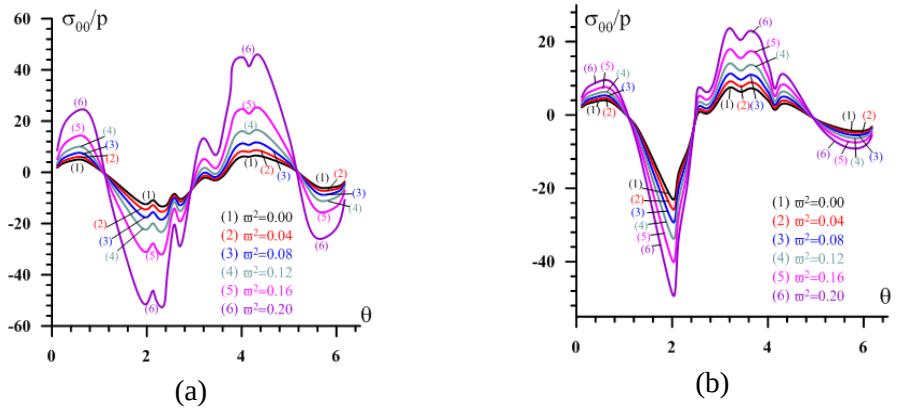

Figure 8: The influence of $\bar{\omega}^2$ on the values of $\sigma_{\theta\theta}/p$ with respect to θ a) for $q/E_1=0$ and b) for $q/E_1=0.005$ in the case where $b/R=22.00$; $c/R=7.75$, $h_U/R=h_A/R=5$, $E_2/E_1=E_3/E_1=0.5$; $G_{12}/E_1=G_{13}/E_1=G_{23}/E_1=0.1$ and $\gamma_{31}=\ell_3/\ell_1=1$.

Fig. 9 shows the influence of E_2/E_1 on the values of $\sigma_{\theta\theta}/p$ for $b/R=22.00$,

$h_A/R=h_U/R=5$, $c/R=7.75$, $G_{12}/E_1=G_{13}/E_1=G_{23}/E_1=0.1$, $E_3/E_1=0.5$ and $\bar{\omega}^2=0.16$. It follows from the graphs that the absolute values of $\sigma_{\theta\theta}/p$ decreases monotonically with E_2/E_1 for both cases where $q/E_1=0$ and $q/E_1\neq 0$.

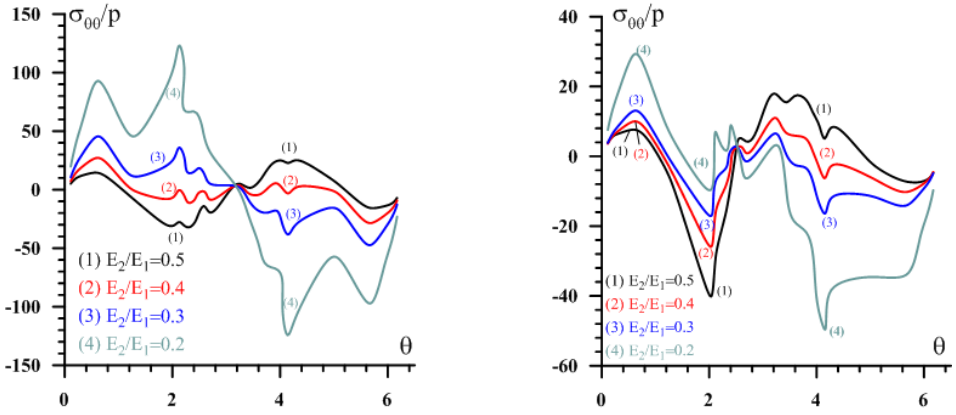

Figure 9: The influence of E_2/E_1 on the values of $\sigma_{\theta\theta}/p$ for $q/E_1=0$ (a) and $q/E_1=0.005$ (b) in the case where $b/R=22.00$; $h_U/R=h_A/R=5$, $c/R=7.75$, $\bar{\omega}^2=0.16$, $G_{12}/E_1=G_{13}/E_1=G_{23}/E_1=0.1$ and $E_3/E_1=0.5$.

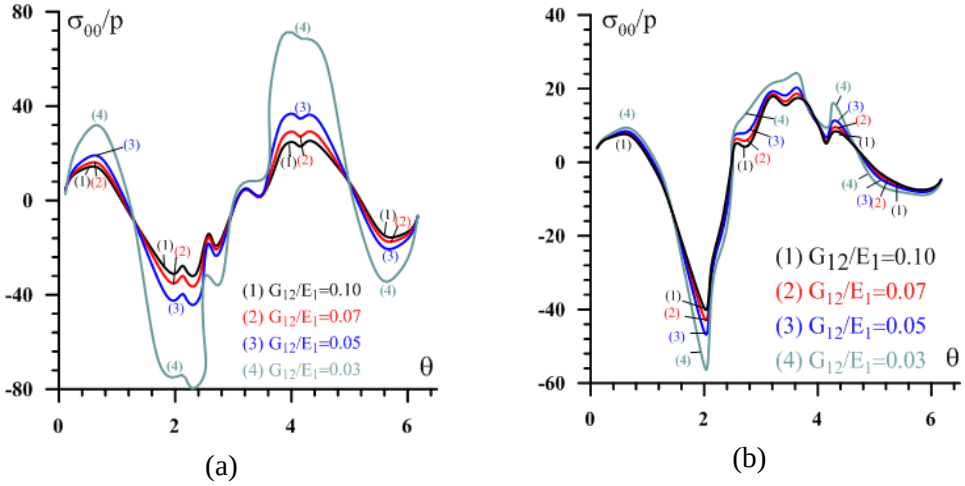

Figure 10: The influence of G_{12}/E_1 on the values of $\sigma_{\theta\theta}/p$ for $q/E_1=0$ (a) and $q/E_1=0.005$ (b) in the case where $b/R=22.00$; $h_U/R=h_A/R=5$, $c/R=7.75$, $\bar{\omega}^2=0.16$, $E_2/E_1=E_3/E_1=0.5$ and $G_{13}/E_1=G_{23}/E_1=0.1$.

Fig. 10 shows the influence of G_{12}/E_1 on the values of $\sigma_{\theta\theta}/p$ in the case where

$b/R=22.00$, $h_U/R=h_A/R=5$, $c/R=7.75$, $\bar{\omega}^2=0.16$, $E_2/E_1=E_3/E_1=0.5$ and $G_{13}/E_1=G_{23}/E_1=0.1$. It follows from the graphs that the absolute values of $\sigma_{\theta\theta}/p$ decreases monotonically with G_{12}/E_1 for both cases where $q/E_1\neq 0$ and $q/E_1=0$.

Fig. 11 shows the influence of the position of the cavities (h_U/R) along the Ox_2 axis on the values of $\sigma_{\theta\theta}/p$ for the case where $b/R=22.00$; $h_A=h-h_U-2R$; $c/R=7.75$, $E_2/E_1=E_3/E_1=0.5$; $G_{12}/E_1=G_{13}/E_1=G_{23}/E_1=0.1$. and $\bar{\omega}^2=0.16$. It follows from the graphs that the absolute values of $\sigma_{\theta\theta}/p$ increases monotonically with a decrease in the values of h_U/R, for the cases where $q/E_1\neq 0$ and $q/E_1=0$.

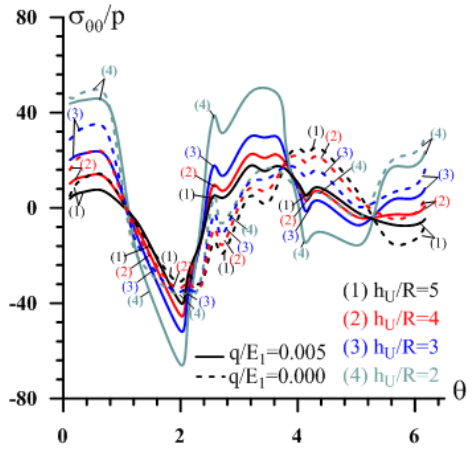

Figure 11: The distribution of $\sigma_{\theta\theta}/p$ with respect to θ under various thicknesses between the upper plane of the cavities and upper face-plane of the plate, i.e. h_U/R in the case where $b/R=22.00$, $h_U/R=h_A/R=5$, $c/R=7.75$, $\bar{\omega}^2=0.16$, $E_2/E_1=E_3/E_1=0.5$; and $G_{12}/E_1=G_{13}/E_1=G_{23}/E_1=0.1$.

Fig. 12 shows the influence of $\gamma_{31}=\ell_3/\ell_1$ on the values of $\sigma_{\theta\theta}/p$ for the case where $q/E_1=0$ and $\bar{\omega}^2=0.08$ (a) and $q/E_1=0.005$ and $\bar{\omega}^2=0.16$ (b), respectively. It follows from the graphs that the absolute values of $\sigma_{\theta\theta}/p$ increases monotonically with $\gamma_{31}=\ell_3/\ell_1$ for the cases where $q/E_1\neq 0$ and $q/E_1=0$ and approach their limit values, i.e. the values determined from the corresponding boundary-value problem in the plane-strain state. These results also confirm the reliability of the algorithm and the PC programs composed and used by the author for determination of the numerical solutions.

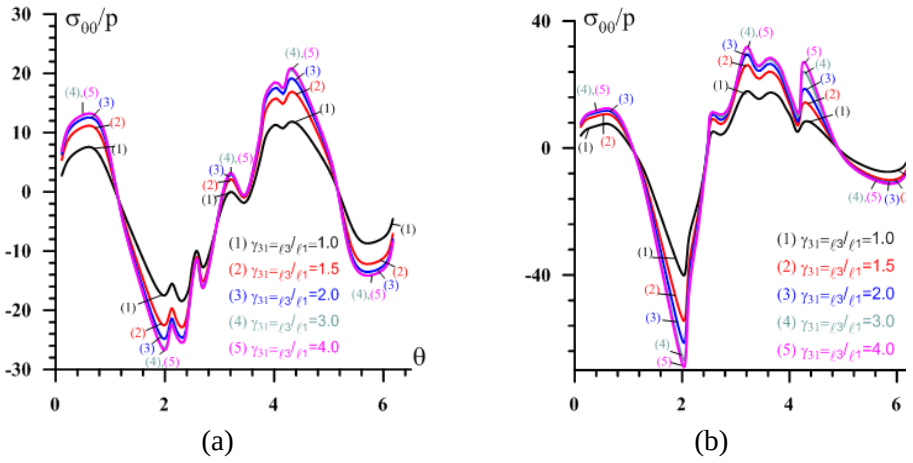

Figure 12: The distribution of $\sigma_{\theta\theta}/p$ with respect to θ under various $\gamma_{31}=\ell_3/\ell_1$ for $q/E_1=0$ and $\bar{\omega}^2=0.08$ (a) and $q/E_1=0.005$ and $\bar{\omega}^2=0.16$ (b) in the case where $b/R=22.00$, $h_U/R=h_A/R=5$, $E_2/E_1=E_3/E_1=0.5$; $G_{12}/E_1=G_{13}/E_1=G_{23}/E_1=0.1$ and $c/R=7.75$.

5 Conclusions

Thus, in the present paper, within the scope of the Three-Dimensional Linearized Theory of Elastic Waves in Initially Stressed Bodies (TDLTEWISB), natural and forced vibration of a rectangular pre-stressed plate containing two neighboring equal parallel cylindrical cavities (lying width-wise in the plate) whose cross sections are rectangular with rounded-off corners has been investigated. It was assumed that the material of the plate is orthotropic. The investigations were carried out by employing 3D FEM modeling. First, the initial stress state caused by uniform stretching forces acting on two end planes of the plate was determined using the linear theory of elasticity. Next, the stress state caused by time–harmonic forces acting on the upper free face plane of the plate was determined. All the end surfaces of the plate are simply supported. Numerical results on the dynamical stress concentrations around the holes and the influence of the orthotropic material properties and the influence of initial stretching on these concentrations, as well as interaction between the holes were presented and compared with the corresponding numerical results for transversely isotropic plate with two cylindrical cavities and for a plate without holes.

From the numerical results obtained, the following inferences can be drawn:

- The values of the fundamental frequency $\bar{\omega}_{cr}^2$ approximate a certain asymptote with a decrease in the total volume of the cavities i.e. with a decrease in the ratio of b/R.
- The values of the fundamental frequency $\bar{\omega}_{cr}^2$ increases with the distance between the cavities.

- The values of $\bar{\omega}_{cr}^2$ are more influenced by the values of G_{12}/E_1 than those of the other shear moduli G_{13}/E_1 and G_{23}/E_1, and decreases with a decrease in the shear modulus $\mathrm{G_{ij}}/\mathrm{E_1}$.
- The values of the fundamental frequency $\bar{\omega}_{cr}^2$ increases (decreases) with the initial stretching (compressing) force i.e. with values of q/E_1.
- The values of the fundamental frequency $\bar{\omega}_{cr}^2$ decreases as the cavities approach the upper free face plane of the plate i.e. with a decrease in the values of h_U/R.
- The dynamic (time harmonic) stress concentration of $|\sigma_{\theta\theta}|/p$ around the cavities decreases (increases) with the initial stretching (compressing) of the plate.
- The dynamic stress concentration of $|\sigma_{\theta\theta}|/p$ decreases monotonically with the distance between the cavities for $(\mathrm{q}/\mathrm{E_1}=0.005)$ but increases slightly with the distance between the cavities for $(\mathrm{q}/\mathrm{E_1}=0)$.
- An increase in the values of the frequency of the external forces causes an increase in the values of the dynamic stress concentration of $|\sigma_{\theta\theta}|/p$.
- The dynamic stress concentration of $|\sigma_{\theta\theta}|/p$ around the cavities decreases with the parameters $\mathrm{E_2}/\mathrm{E_1}$.
- The dynamic stress concentration of $|\sigma_{\theta\theta}|/p$ around the cavities decrease with the parameters $\mathrm{G_{12}}/\mathrm{E_1}$.
- The dynamic stress concentration of $|\sigma_{\theta\theta}|/p$ around the cavities increases monotonically with $\gamma_{31}=\ell_3/\ell_1$ and approaches a certain limit value, i.e. the value which is determined from the corresponding boundary-value problem in the plane-strain state.

Acknowledgement: The author is grateful to Prof. Dr. Surkay D. AKBAROV for comments and discussions and Prof. Dr. Nazmiye YAHNIOGLU for considerable revision of the manuscript.

References

Akbarov, S.D.; Guz, A.N. (2000): *Mechanics of Curved Composites*, Kluwer Academics Publisher, Dordrecht.

Akbarov, S.D.; Yahnioglu, N.; Babuscu Yesil, U. (2010): Forced Vibration of An Initially Stressed Thick Rectangular Plate Made of an Orthotropic Material with A Cylindrical Hole, *Mech. of Comp. Mat.*, vol.46, no.3, pp.287-298.

Akbarov, S.D.; Yahnioglu, N.; Babuscu Yesil, U. (2012): 3D Analysis of the forced vibrations of a prestressed rectangular composite plate with two neighboring cylindrical

cavities, *CMC (Computers, Materials & Continua)*, vol.28, no.2, pp147-164.

Akbarov, S.D.; Yahnioglu, N.; Babuscu Yesil, U. (2012) : 3D FEM Analysis of Stress Concentrations Around Two Neighboring Cylindrical Holes Within a Pre-Stressed Rectangular Composite Plate Under Bending, *Mech. of Comp. Ma.*, vol.48, no.5, pp. 499-510.

Chaudhuri, R.A. (2007): Weakening Effects of Internal Part-Through Elliptic Holes in Homogeneous and Laminated Composite Plates, *Composites Structures*, vol.81, pp. 362-373.

Christensen, R.M. (1979): *Mechanics of Composite Materials*, John Willey and Sons, Int. New York.

Guz, A.N. (2004): *Elastic waves in bodies with initial (residual) stresses*. "A.C.K.", Kiev.vol.

Khoma, I.Y.; Kondratenko, O.A. (2008): Stress distribution around a circular cylindrical cavity in a prestressed plate, *International Applied Mechanics*, vol.44, no.1, pp.23-33.

Kwaka, M.K.; Han, S. (2007): Free vibration analysis of rectangular plate with a hole by means of independent coordinate, coupling method, *J. Sound Vibr*, vol.306, pp. 12-30.

Nagpal, S.; Jain, N.; Sanyal, S. (2012): Stress concentration and its mitigation techniques in flat plate with singularities-a critical review, *Eng. Jour.*, vol.16, no.1, pp.1-15.

Savin, G.N. (1961): *Stress Concentration Around Holes*, E. Gros Translator, Pergomon.

Sivakumar, K.; Iyengar, N.G.R. (1999): Free vibration of laminated composite plates with cutout, *J. Sound Vibr.*, vol. 221, no.3, pp.443-470.

Toubal, L.; Karama, M.; Lorrai, B. (2005): Stress concentration in a circular hole in composite plate, *Composite Structures*, vol.68, no.1, pp.31-36.

Yahnioglu, N. (2007): On the stress distribution in the pre-stretched simply supported strip containing two neighbouring circular holes under forced vibration, *Int. Appl. Mech.*, vol.43, no.10, pp.135-140.

Yahnioglu, N.; Babuscu Yesil, U. (2009): Forced vibration of an initial stressed rectangular composite thick plate with a cylindrical hole, *ASME 2009 International Mechanical Engineering Congress and Exposition IMECE09*, November 13-19, Lake Buena Vista, Florida, USA.

Zhen, W.; Wanji, C. (2009): Stress analysis of laminated composite plates with a circular hole according to a single-layer higher-order model, *Composite Structures*, vol.90, pp. 122-129.

Zheng, Y.; Chang-Boo, K.; Chongdu, C.; Hyeon, G.B. (2008) : The concentration of stress and strain in finite thickness elastic plate containing a circular hole, *International Journal of Solids and Structures*, vol.45, no.3-4, pp.713-731.

Zienkiewicz, O.C.; Taylor, R.L. (1989) : *The Finite Element Methods: Basic Formulation and Linear Problems*, vol.1, 4th Ed., Mc Graw-Hill Book Company, Oxford.